Prediction Model And Experimental Study Of Wind Speed Effect On The Tall Buildings Using Machine Learning

Hassan Ahmed [a], Eman Elnos Aly [b], Mostafa E.A. Elsayed [c], Mohamed A. Khalifa[d], M. A. Aziz [e], Osama A. Gaheen [f]

Abstract
The scope of this study, It provides the designer with the best cross section shape for the building that achieves the minimum drag force and the best natural ventilation for the building. A total of 8 shapes of tall buildings models are experimentally studied in present work to study the aerodynamic effect through measuring and visualization of important aerodynamic parameters and flow around the models. The study utilizes computational fluid dynamics (CFD) solver to simulate different cross section of building models subjected to three different wind speeds 10, 20 and 30 m/s. The shapes of high-rise buildings have a strong effect on the drag forces on the building and the wind environment surrounding the building, as this affects ventilation as well, especially those located in a strong wind environment. The ascending order ranking of the building models showed minimum and maximum drag force associated with circular cross section with ribs (model A-2) and rectangular cross section (B-1). The reduction in drag force percentage at velocity 30 m/s equals 91.59% due to addition of ribs to circular cross section (model A-1). The drag force increases for all investigated building models as air velocity increases from 10 to 20 to 30 m/s. The pressure values around the surface of the building were measured and studied in order to explain the change in Drag forces and predict the best cross section from a ventilation point of view.
Key Words; *tall building, wind effect, machine learning*

I.   Introduction

Numerous tall buildings are already being constructed or developing all around the world. Peoples are migrating to urban areas now-a-days. In order to accommodate such big population in cities, many lands are occupied by the building authorities for the construction of high-rise building projects. Construction of these high-rise structures becomes difficult when available land have many irregularities in terms of size and shape. For structural design, the main lateral loads considered are typically wind and seismic [1] and [2].

The structure is permitted to yield, in seismic design, to introduce inelastic behavior. On the other hand, only elastic behavior is permitted in the strength design of conventional wind design codes. The following issues are commonly raised when the structure is designed to yield under wind loads:

(1) Relatively low level of loads com- pared to actual seismic loads.
(2) Fatigue failure by long duration of loading.
(3) Ratcheting by the mean component of wind load.
(4) Fluid-structure-interaction by large deformation (i.e., aerodynamic instability problem).

The difference in design philosophy causes complications in the design of high-rise buildings for wind and seismic loads. With the development of construction techniques and improvement of the properties of building materials, it has become functional to build very tall, light, and slender buildings. This causes more sensitivity to wind loads as tall buildings become more flexible with lower damping [3] and [4]. One of the most important factors that govern the design of a tall building is the wind load. High-rise building structures and facades are highly vulnerable to wind loads [5].

With this respect, designers have to take into account the required structural performance of buildings in terms of survivability, serviceability, and habitability as well as keeping the motions of towers within comfortable limits [6]. A wide range of factors affect the level of wind pressure on tall buildings such as building height, shapes, and dimension, surrounding environment, and wind characteristics. Furthermore, fluctuating wind can lead to building vibration and may cause local or overall damage [7]. A building structure, under the action of wind, experiences two types of forces namely drag and lift, and torsional moments. The drag force is experienced along the direction of flow and the lift occurs perpendicular to it [8]. The along-wind motion primarily results from pressure fluctuations on the windward and leeward faces and generally follows fluctuations in the

approaching flow. Thus, the crosswind forces act perpendicular to the direction of mean wind flow and its common source is associated with "vortex shedding [9]. Ultimately, the torsional motion occurs due to an imbalance in the instantaneous pressure distribution on each face of a building [10].

There are several different ways used by engineers and architects to reduce the effect of wind load on tall buildings such as stiffening, adding mass, or supplementary damping systems [11]. There are also aerodynamic methods for mitigation of wind loads on buildings like global and local aerodynamic modifications [12]. In line with this concept, one important way to achieve a reduction in wind- induced loads on buildings is to use an aerodynamic design of building shapes which also is one of the effective ways for mitigating lateral wind forces [5]. However, as the tall building design practice is recently driven by exotic and more complex forms [13]. It is recommended to design buildings with more streamlined shapes in order to reduce the buffeting load against buildings. In addition, self-induced vortex shedding loads can be alleviated through modifications in a building basic plan shape or a more three-dimensional design on the upper level [14].

Due to several variable conditions, wind action over a building is quite difficult to predict. The variables are: building size and shape, surrounding terrain conditions, relative distance between the principal building and the interfering building and wind direction. These variable conditions may either slow down or accelerate the wind effect in certain regions. The interference effects between high-rise buildings have been studied for many decades by many researchers [15] and [16]. Wind effects on high-rise structures have been investigated by many researchers using wind tunnel test like Nagar et al [17] executed an experimental study on "H" shaped high rise buildings. Kwok [18] investigated the wind induced response on the various shape of tall buildings. Blessmann and Riera [19] performed the test in wind tunnel and obtained the wind induced response on the interfering tall buildings. Pal et al [20] performed the experiment in boundary layer wind tunnel on square plane shape model and remodel triangle shape model of high rise structure.

In the realm of wind engineering, ANN-based forecasts of wind pressure features are receiving more and more attention. Three ANN models—BPNN, GA-BP, and WNN—were trained with study test data from a wind tunnel. The time series, power spectra, and distribution characteristics of wind pressure were reconstructed using these models [21].

The scope of this study, a designer who designs a tall building needs to choose a geometry as the base plan shape of the building as it affects the overall geometry of the building. So, a careful selection of a suitable geometry is critical and a good knowledge of the geometries and their behavior, against high wind speeds, seems to be imperative. This study aims to investigate the aerodynamic design and the effects of wind on tall structures under different geometric plan configurations of tall buildings having the same parameters. Furthermore, it is intended to study the behavior of the tall structures when subjected to strong winds in along-wind and crosswind directions. Hence, a total of 8 shapes of tall buildings models are used in present work to study the aerodynamic effect through measuring and visualization of important aerodynamic parameters and flow around the models. The study includes simulation of different cross section of building models at three different wind speeds 10, 20 and 30 m/s.

In addition, we have created a model of artificial intelligence based on neural networks that can forecast weather effects caused by wind speed on skyscrapers as well as the variations in those effects depending on the design of the shape of the buildings.

II.   Test Rig and Experimental Set Up
Wind tunnel and test equipment

There are many cases where using analytical methods is difficult to predict certain types of wind loads and associated structural response. For example, when the aerodynamic shape of the building is rather uncommon or the building is very flexible so that its motion affects the aerodynamic forces acting on it. In such situations, more accurate estimates of wind effects on buildings can be obtained through aero elastic model testing in a wind tunnel. Wind tunnel testing is now common practice for design of most tall buildings. In many cases, owners of proposed moderately tall buildings are also encouraged to allow for wind tunnel testing, as the costs associated with such testing can be offset by the substantial savings in the building costs, due to the reduced design wind loading.

Test section and experimental setup

Figure 1 shows the wind tunnel used in the current study. The driving speed inside the test section ranges from 0 to 35 m/s, and the desired speed is controlled through the operating indicator. The speed is measured inside the test chamber using a pitot static tube and a digital manometer. The dimensions of the test section are $46 \times 47 \times 121$ cm^3.

Figure 1 Wind tunnel used in the current study.

The experimental setup comprised several components, such as a load cell capable of supporting up to 40 kgf, a digital manometer and a pitot static tube whose technical specifications are listed in Table 1. The velocity was measured using a pitot static tube anemometer. The experiment was conducted within a Reynolds number (Re) range of 0.5×10^5 to 1.4×10^5 based on the model characteristic length. The aerodynamic forces measuring device was calibrated at the National Institute for Standards (NIS) in Egypt. Where the an average error in measurements does not exceed 0.76% .

Table 1 Measuring devices characteristics

No.	Device	Specification	
1	**Digital manometer** Measured quantity pressure	Resolution	9.5×10^{-4} atm
		Range	0:23.8 atm
		Accuracy	±0.25% reading
2	**Pitot tube**	Resolution	0.01 m/s
		Accuracy (Air velocity)	±5 % ±1 digit
		Measurement quota	approx. 0.8 s
		Display	LCD (46.7 x 60 mm)
3	**Drag force measuring device (weight kg)**	Resolution	1 gm
		Range	0: 40 kg
		Accuracy	±0.7% reading

Test section wind speed

At great heights above the surface of the earth, where frictional effects are negligible, air movements are driven by pressure gradients in the atmosphere, which in turn are the thermodynamic consequences of variable solar heating of the earth. This upper-level wind speed is known as the gradient wind velocity. In practice, it has been found useful to start with a reference wind speed based on statistical analysis of wind speed records obtained at meteorological stations throughout the country. The definition of reference wind speed varies from one country to another. Contour maps of reference wind speeds that apply for nominated statistical Return Periods in various countries are usually available.

A three wind speeds are used during current experimental investigation which simulates the different levels of wind speed in real life represents low , medium and high wind speeds. Table 2 shows the values of wind speeds considered in the present work.

Table 2 Wind speed values considered in the present work

Case	Wind type	Wind speed (m/sec)
1	Low	10
2	Medium	20
3	High	30

Figure 2 shows the model being installed inside the test section and mounted on a load cell to measure the drag forces acting on the model through a digital screen connected to the load cells. The distribution of pressures on the model surfaces is also measured using a digital manometer. These measurements are used to

determine the locations of the vortices resulting from the shape which directly effect on the ventilation of the building model.
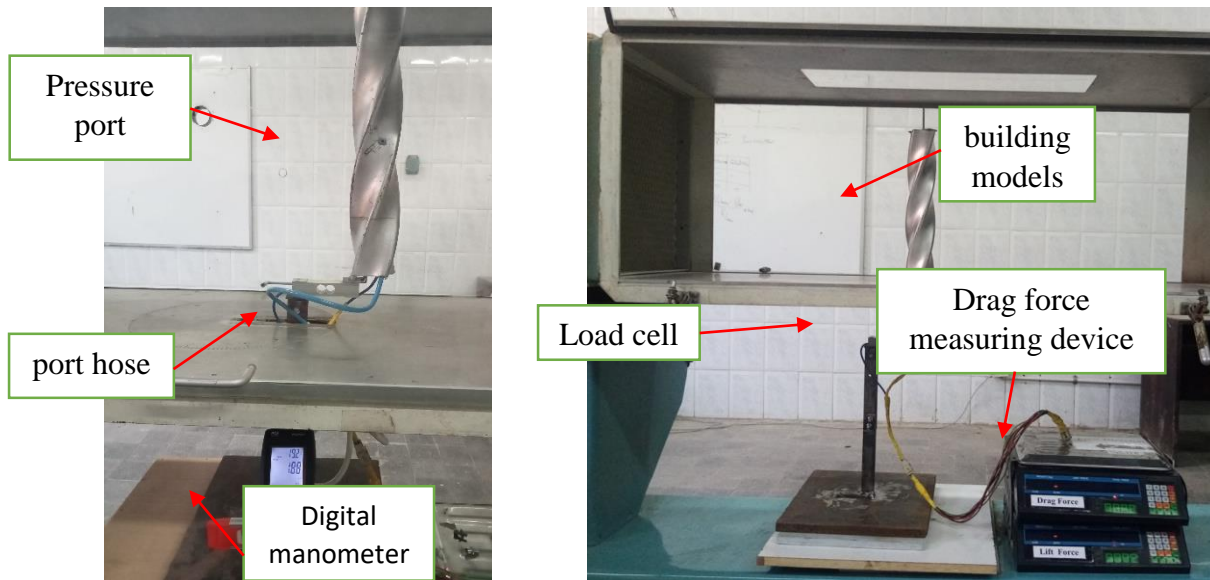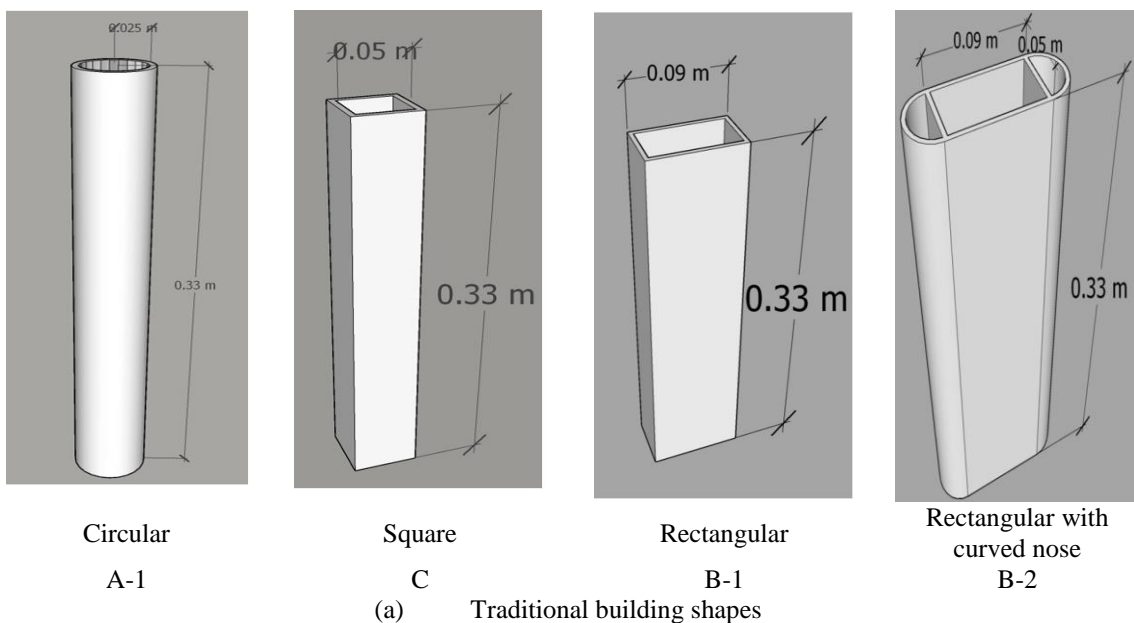

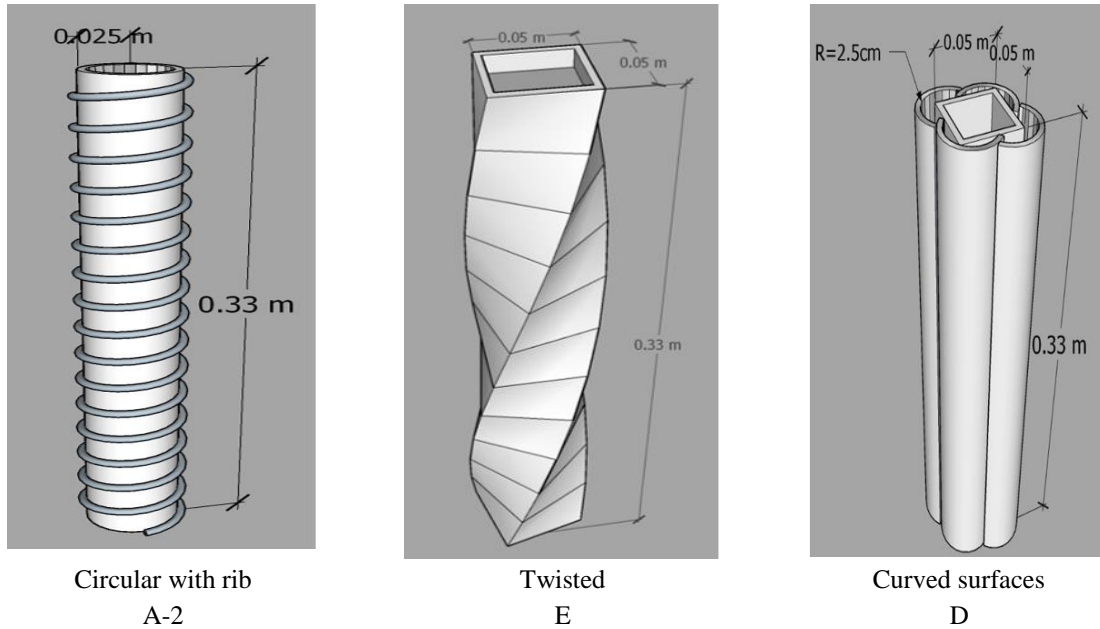**Figure 2 Building model set up**

Building Shapes Models

Experimental building models were categorized into two groups with different shapes namely traditional and modern building shapes. The different shape are listed in Table 3. The building models CAD diagrams are shown in Figure 3. The actual building models are shown in Figure 4.

Table 3 different shapes

Case	Cross Section	Model shape
A-1	Circular	Traditional
C	Square	
B-1	Rectangular	
B-2	Rectangular with curved nose	
A-2	Circular with rib	Modern
E	Twisted	
D	Curved surfaces	

Circular	Square	Rectangular	Rectangular with curved nose
A-1	C	B-1	B-2

(a)   Traditional building shapes

Circular with rib

A-2

Twisted

E

Curved surfaces

D

(b) Modern building shapes

Figure 3 The building models shapes CAD diagram

Circular

A-1

Square

C

Rectangular

B-1

Rectangular with curved nose

B-2

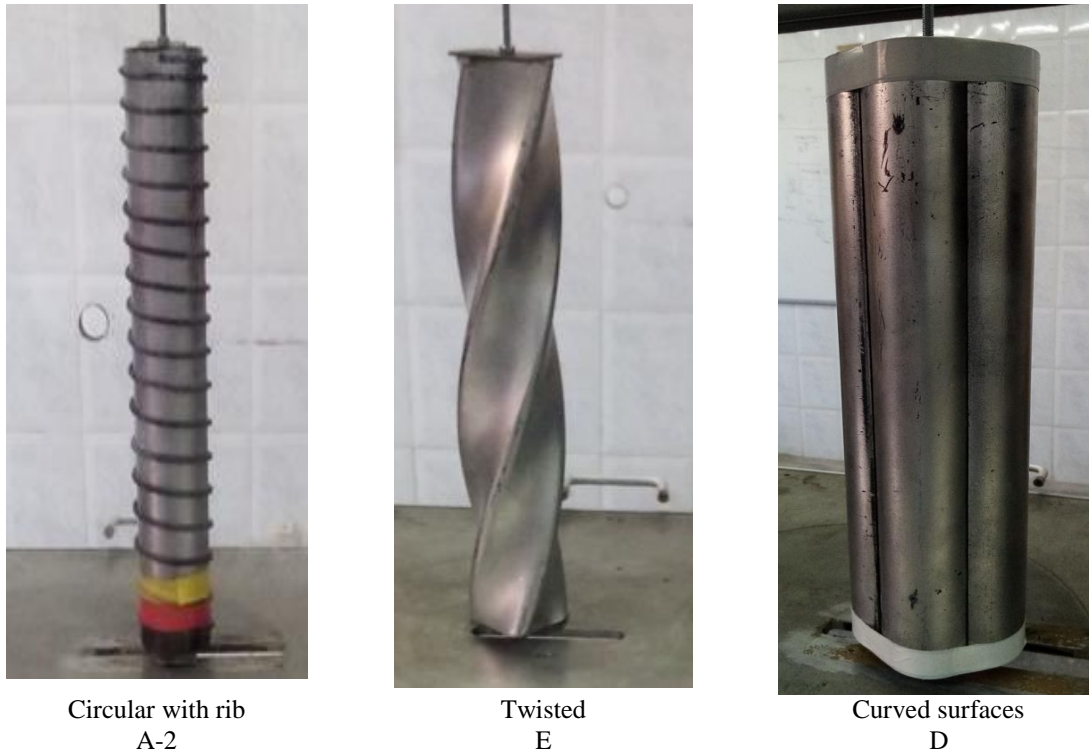| Circular with rib | Twisted | Curved surfaces |
| A-2 | E | D |
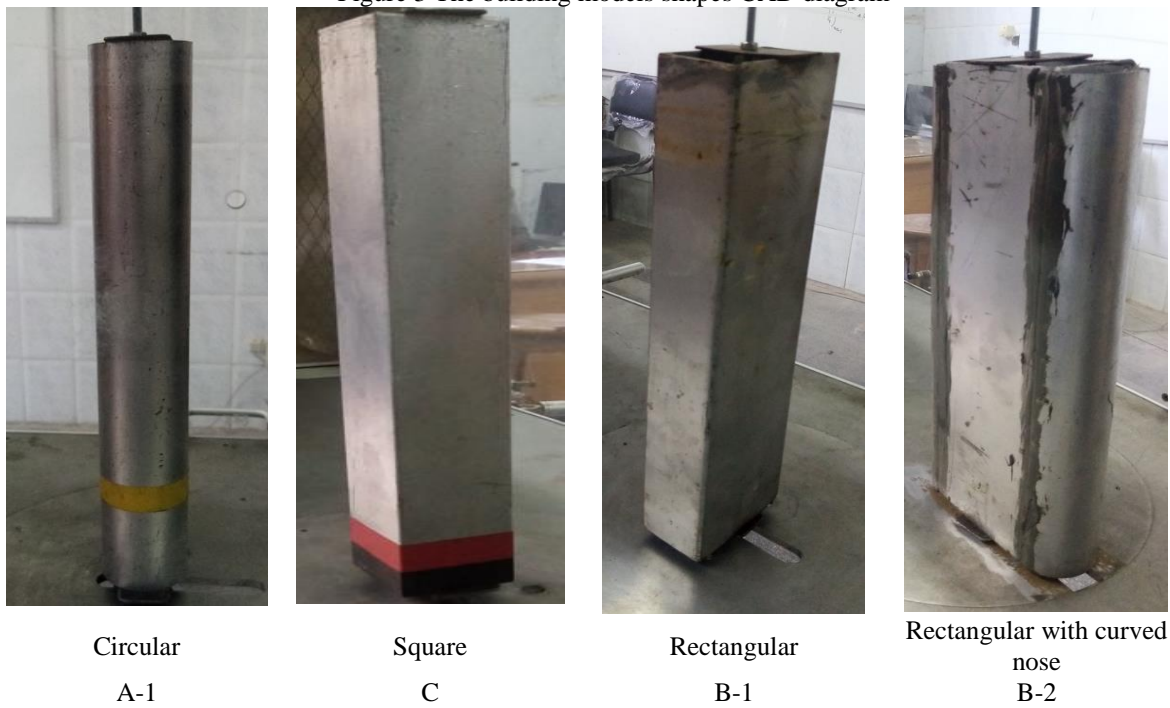
Figure 4 The building models shapes true models

Artificial neural network Model

The main experimental variables that needed to be represented using artificial neural networks were the aerodynamic properties of skyscrapers that used, two configurations of drag force, and building forms. Experimental findings were gathered and recorded. The feed forward, which is commonly utilized in many studies, is a type of multiple layer perceptron that consists of input, hidden, and output layers with a specific number of neurons in each layer, initial weights and biases, as well as neuron functions. The summation function and the activation function are carried out by the neuron in each layer to add the weighted inputs and produce the output as shown in figure 5.
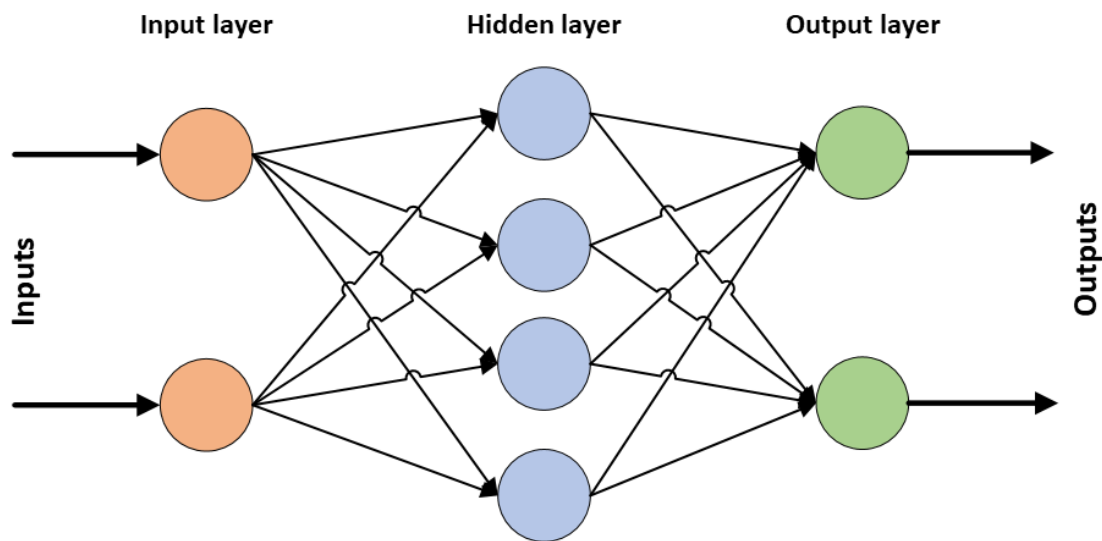

Figure 5. The Feed-forward Neural Network perceptron.

Wind speed (V) and building models make up the input layer, while drag coefficient (C_D) and surface pressure (P) make up the output layer as shown in figure 6. To verify the model's validity, all input data sets were divided into train and test data sets. Seventy percent of the data sets were chosen for training to create the neural

network, while the remaining data points were chosen for the test data set and validation. During training, the weights and biases of the network are adjusted in an effort to reduce the objective function, or error function. MSE is a well-liked metric to use in this context.
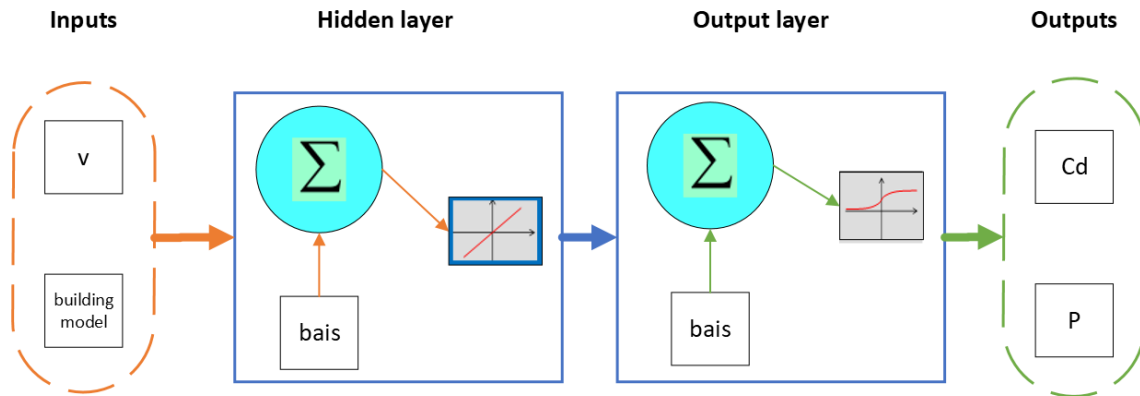

Figure 6 The ANN structure for predicting the C_D and P

In this experiment, 150 data samples were used to observe the effects of wind speed, building models, and surface pressure on drag force characteristics.

For the training, validation, and testing phases of C_D employing ANN, regression plots for the network outputs relative to the objectives (actual outputs) were shown in Figure 7 in order to evaluate the performance of the established network. A better correlation between network findings and actual outputs was indicated by graphs with higher regression (R) values.
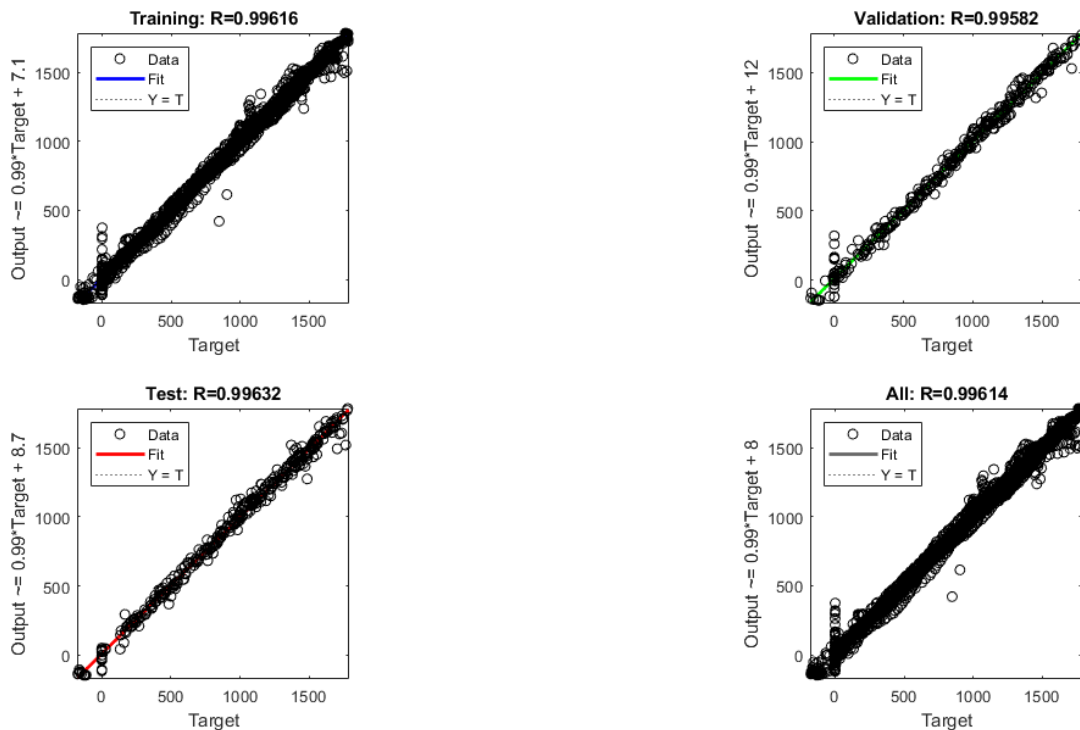

Figure 7 The validation data of neural network training set.

III.   Wind effects and aerodynamics calculations

Governing equations

Drag coefficient of any conventional configuration

$$C_D = \frac{D}{q_\infty S} \tag{1}$$

where D is the drag force in N, S is the frontal area per unit span and q_∞ is the dynamic pressure in Pa
The Reynolds number is based on the building model diameter d.

$$Re = \frac{\rho_\infty V_\infty d}{\mu_\infty} \tag{2}$$

Where V_∞ is the wind speed in m/s , ρ_∞ is the air density inside the test section in kg/m³ and μ_∞ is the dynamic viscosity in Pa.s

Since these bodies are at zero angle of attack, the drag is equal to the axial force. Hence, the drag per unit span can be written as,
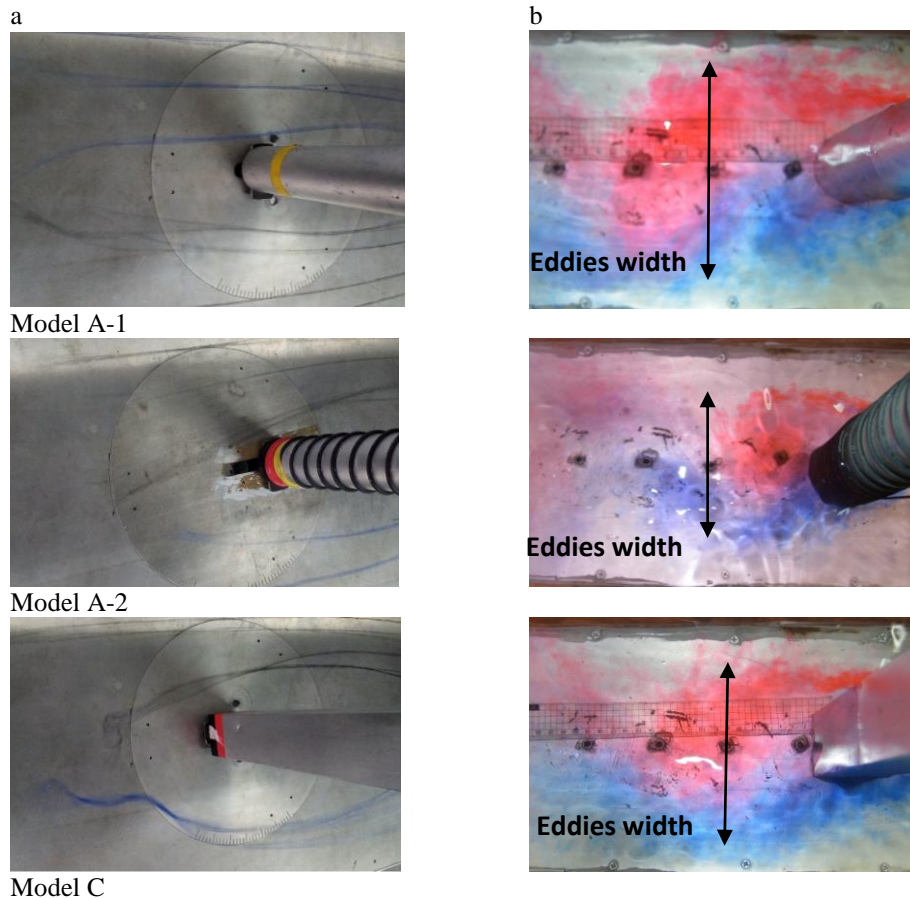
$$D = \int_{LE}^{TE} -P_u sin\theta \, d \, S_u + \int_{LE}^{TE} -P_l sin\theta \, d \, S_l + \int_{LE}^{TE} -\tau_u cos\theta \, d \, S_u + \int_{LE}^{TE} -\tau_l cos\theta \, d \, S_l \tag{3}$$

Where P is the pressure in Pa, τ is the surface shear stress in Pa and S is the elemental surface area in m².

That is, the drag on any aerodynamic body is composed of pressure drag and skin friction drag. Referring to the CFD simulations were used to visualizes the flow field around the building model shapes.

Flow visualization behind building models

The building in the wind environment is exposed to a stagnation pressure in the front surface. On the other side, it is exposed to a vortex zone on both sides and behind the building. The shape and cross section of the building directly affects the flow of the fluid around the building. Figure 8 shows the size and location of the vortices surrounding the building for different cross sections. It also shows the visualization of flow through the use of air inside a wind tunnel by representing the air streams around the building using colored strings. The eddies of water flowing around the different cross section were also observed by dyeing the water by different colors to illustrate the areas of eddies on both sides of the building and the extent of their turbulence behind the building. The visualization results showed that the width of the vortices changed with the changing shape of the building cross section. The eddies zone width behind the building model equal to 2.8d, 1.8d, 3.25d, 2.4d and 1.0d for A-1, A-2, C, E and D respectively where d equals 5 cm.
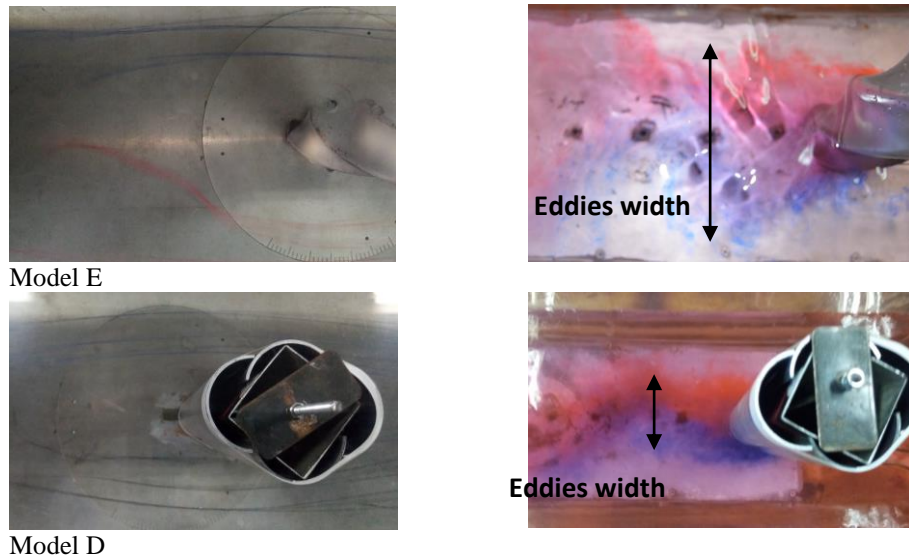
a

Model A-1

b

Eddies width

Model A-2

Eddies width

Model C

Eddies width

Model E

Eddies width

Model D

Eddies width

Figure 8 Stream line visualization in (a) wind tunnel and (b) water tunnel

Flow field analysis around building models

Numerical simulations were performed using a commercial Navier–Stokes flow solver (CFDRC). This package has been used in many different applications in the field of internal and external flows. Three modules from the solver package were used during the current simulations. The geometry and grid generation were performed in the CFD-GEOM module, whereas CFD computations were conducted in the CFD-ACE module. The postprocessing was running in the CFD-VIEW module. Most of the modules are controlled using Python script files. The CFD-ACE multi-physics module is a pressure-based solver. The code solves the time-dependent, Reynolds-averaged Navier–Stokes equations using finite volume, structured grids for turbulent, compressible flows. Spatial accuracy is nominally second-order upwind formulation. The standard k-ε model has been used during the current study.

Wind speed effect on flow field velocity

Figure 9 shows the velocity contours of the flow field around models A-1, B-1 and C. The results indicated identical eddies structures from the location and shape point of view for the same building model cross section at different wind speeds 10, 20 and 30 m/s. Noting the change in velocity magnitude values around the building. On the other hand, by comparing the circle cross section with the rectangular and square cross sections, it becomes clear that the eddies zone extends behind the building, as well as on both sides of the building in the case of the rectangular and square shapes, because of reverse flow. The flow separation area on the two side surfaces in the rectangular cross section are longer than that in the square cross section and almost disappeared in the circular cross section.

Model A-1
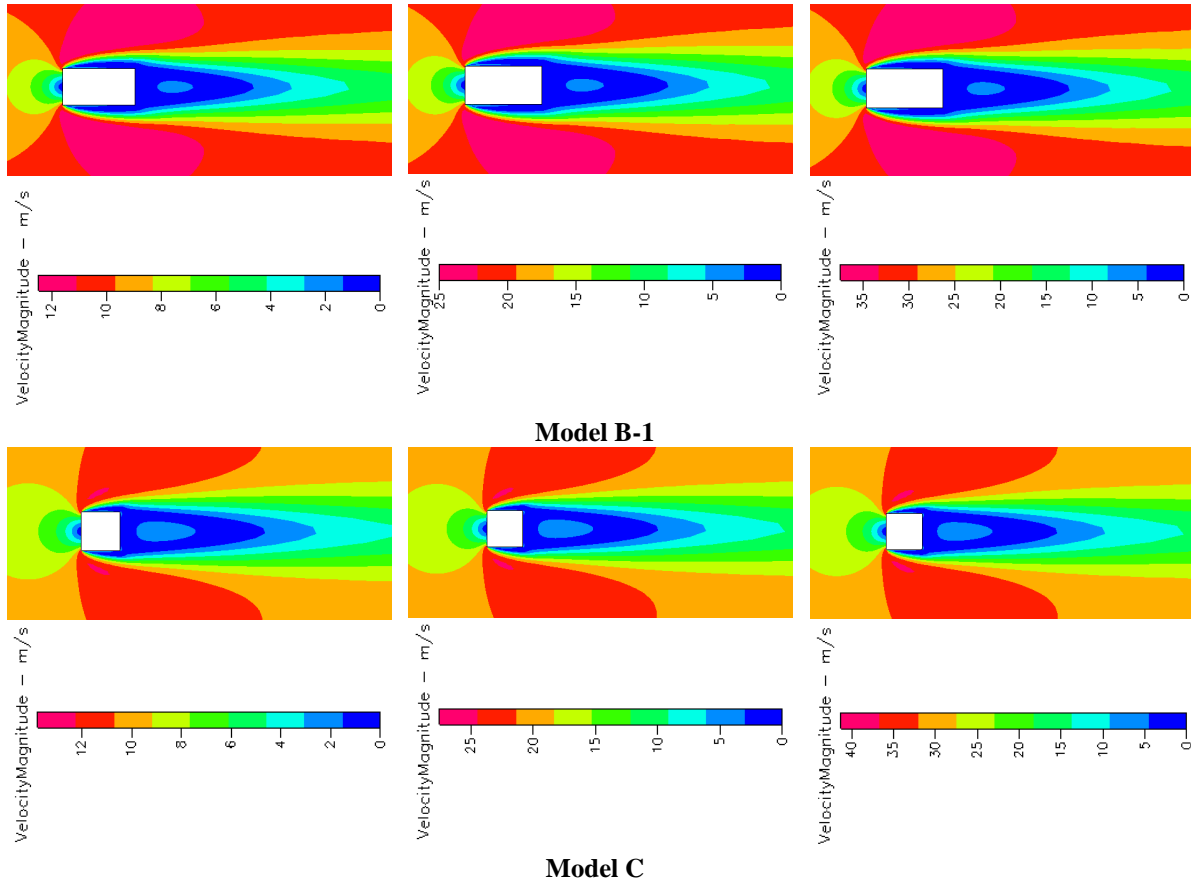
Model B-1
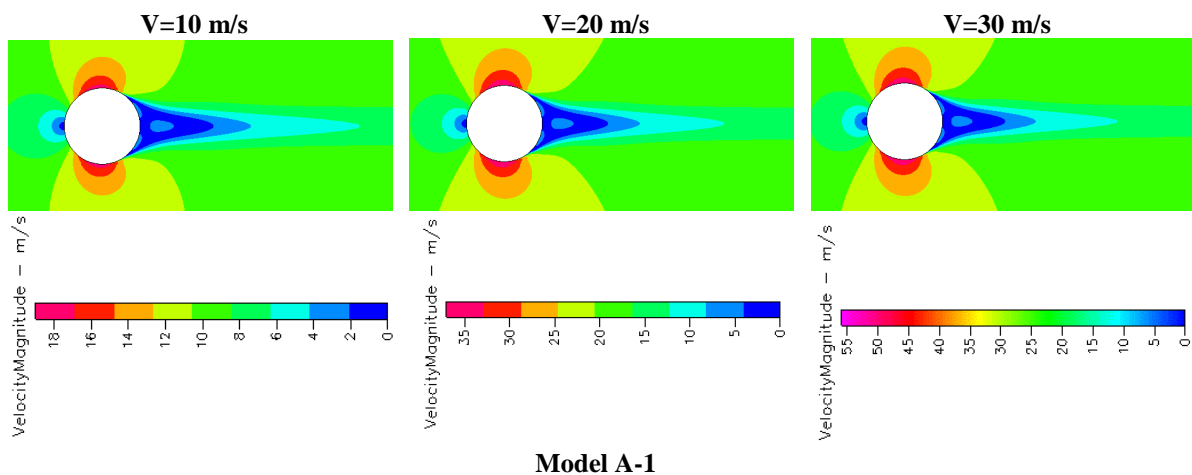
Model C
Figure 9 velocity contours in (m/s)

Wind speed effect on flow field pressure

Figure 10 shows the pressure contours of the flow field around models A-1, B-1 and C. The results show a clear change in the pressure on the upstream surface of the building model. As change from C to B-1 to A-1 the draft flow increase due to little decrease in pressure on the two building side surfaces. The aft eddies behind the building model decreases the pressure. The zone of eddies increases from A-1 to C to B-1. The largest eddies zone is associated with the rectangular cross section building model. The air velocity effect is clear and gives significant variation in pressure values. Increasing the air velocity increases the pressure behind the model A-1. On the other hand, the pressure variation is negligible as increase air velocity for models B-1 and C.
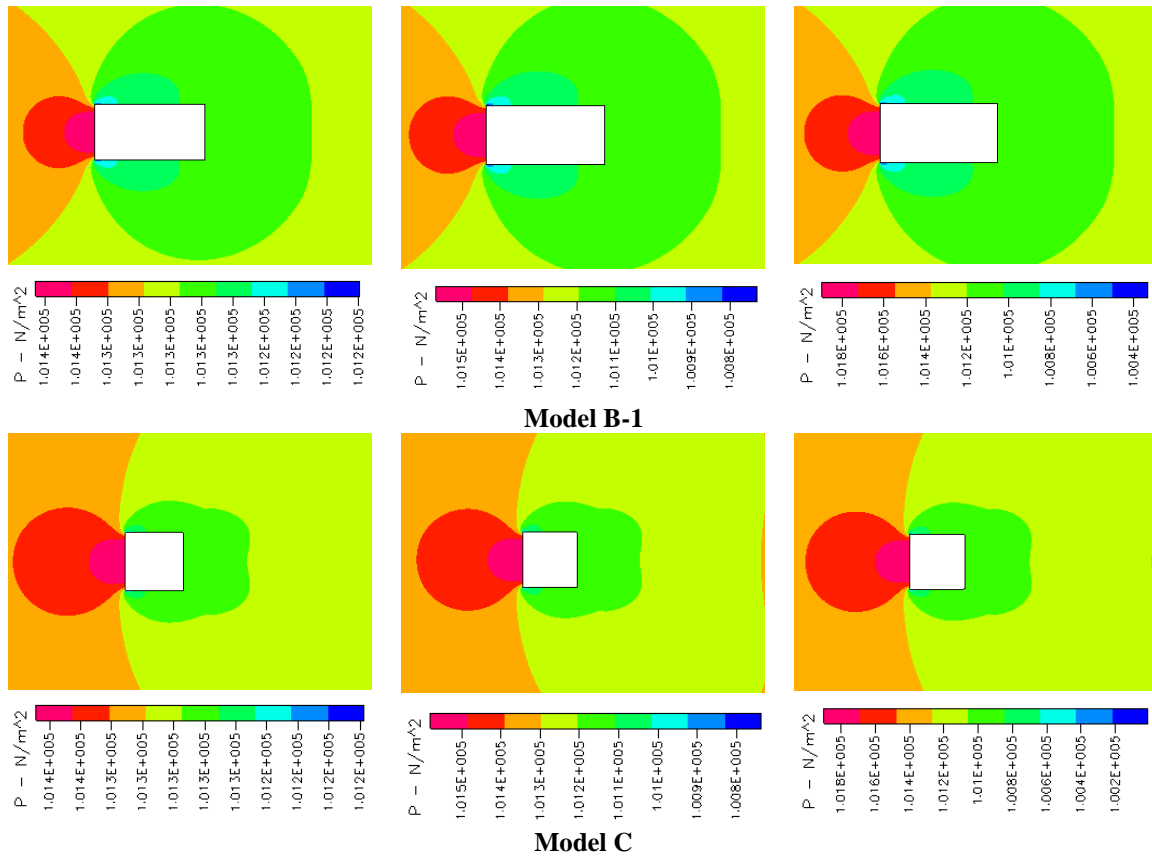
| **V=10 m/s** | **V=20 m/s** | **V=30 m/s** |

Model A-1

Model B-1

Model C
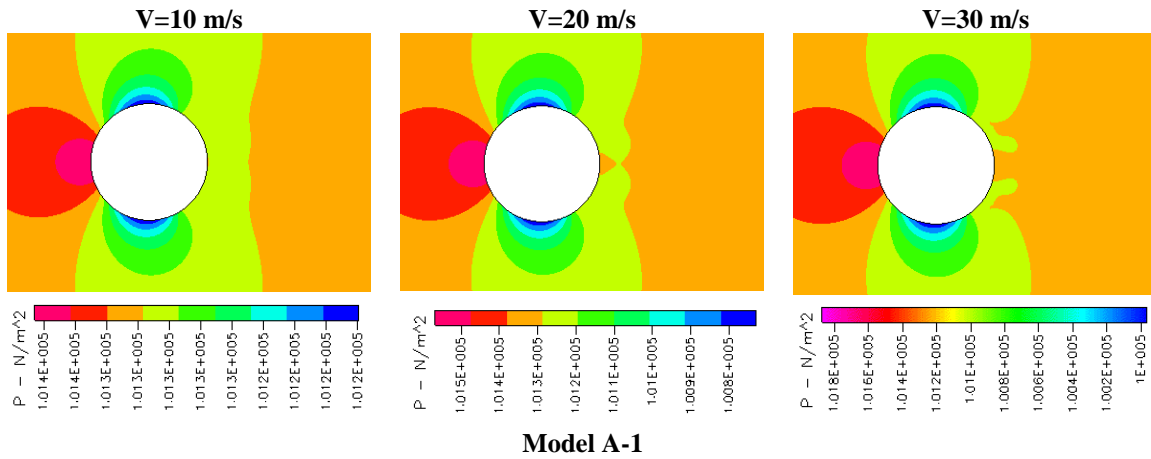
Figure 10 pressure contours in (N/m²)

Experimental errors analysis

Uncertainty analysis is the most significant features to consider when performing experimental work. The instruments used, measurement alteration, and calibration errors are the primary bases of this analysis. The accepted value of uncertainty shifts for low-risk engineering applications is 5 %. The lower this value, the better the results. To calculate the uncertainty value, use the Holman formula presented in Eq. (4) [22]:

$$\omega_x = \sqrt{\left(\frac{\partial X}{\partial x_1}\right)^2 \omega_{x1}^2 + \left(\frac{\partial X}{\partial x_2}\right)^2 \omega_{x2}^2 + \cdots + \left(\frac{\partial X}{\partial x_n}\right)^2 \omega_{xn}^2} \qquad (4)$$

where ω_x is the uncertainty of the parameter X, ω_{xn} is the uncertainty of parameter x_n, and $\frac{\partial X}{\partial x_1}$ is the partial derivative of X concerning x_1. Applying the governing equation to drag, pressure and wind speed and accounting for errors in measurement parameters and devices as shown in Table 1, the uncertainty in drag force measurements is around 0.7 % and in surface pressure around the building is 0.25% which is acceptable for similar aerodynamics applications.

IV.   Results and Discussion
Wind speed effect on the building model drag force

Figure 11 presents the drag force for all investigated building models at different velocity equals 10, 20 and 30 m/s. Figure 11 (a) shows reduction in drag force from 0.714 to 0.06 kg at velocity 30 m/s with reduction percentage 91.59% due to addition of ribs. The decrease in drag force with the same ratio approximately is noticed at air velocities 10 and 20 m/s. Figure 11 (b) presents also reduction in the drag force on the building model B-1 due to addition of curved nose B-2. The reduction percentage in drag force approximately 52.74%. Figure 11 (c) shows the drag value 0.166, 0.676 and 1.360 kg at air velocities 10, 20 and 30 m/s respectively for square cross section building model C. with a modification for model C through addition of twist (model E) or curved surface (model D) the values of drag force reduces with noticeable values as presented in Figure 11 (d) and (e). Figure 11 (f) gives sensible comparison between all experimental building models used in the present work. The ascending order ranking of the building models regarding the drag force was A-2, A-1, D, E, B-2, C and B-1.
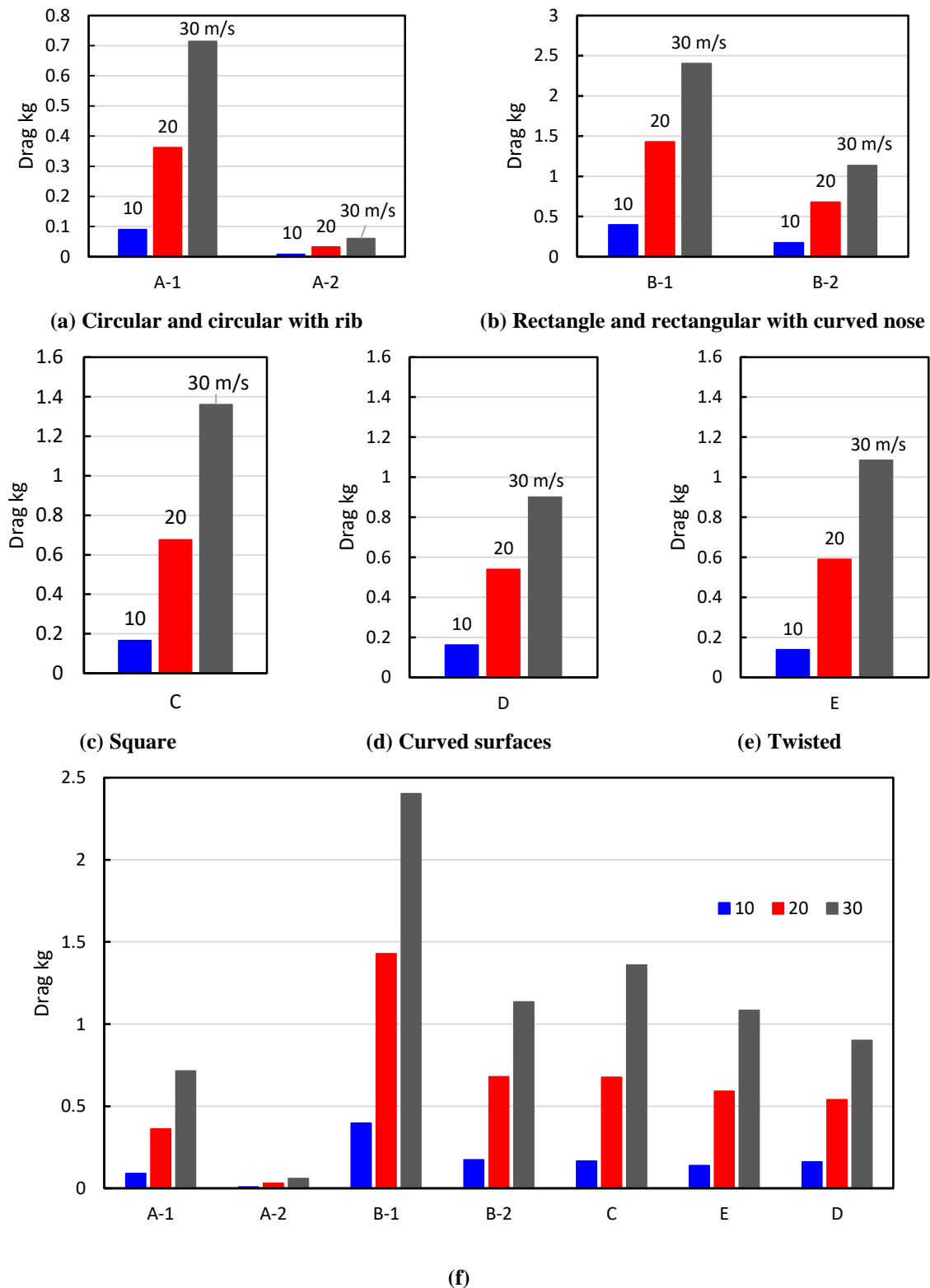
(a) Circular and circular with rib

(b) Rectangle and rectangular with curved nose

(c) Square

(d) Curved surfaces

(e) Twisted

(f)

Figure 11 comparison between drag force for different building models shapes

Wind speed effect on the building surface pressure

The surface pressure was measured using digital manometer connected to the measuring ports. The ports were distributed around the building model at four sides A, B, C and D as shown in Figure 12 for the circular cross section (A-1). They located at the upstream or stagnation point, downstream and two sides of the building model. The measured values are presented in Table 4 for the three wind speeds 10, 20 and 30 m/s. Figure 12 shows the variation of surface pressure at the four sides with the variation in wind speed. The results indicated

that as the wind speed increases, the pressure at stagnation point for the upstream surface also increases. On the other hand, with increasing the wind speed the pressure decreases for the rear and sides surfaces of the model. The building model subjected to positive gage pressure on the upstream surface only. While at the other sides the surface gage pressure was negative. The difference in pressure values between the upstream and downstream is responsible for the drag force on the building model. The pressure at the building model side is responsible for the ventilation movement of the building and the eddies generated around the building.

Table 4 surface pressure variation with wind speed for model A-1

| Wind velocity (m/sec)	Pressure (Pa)			
	Front A	Side B	Rear C	Side D
10	22	-180	-188	-180
20	47	-485	-497	-485
30	89	-944	-924	-944
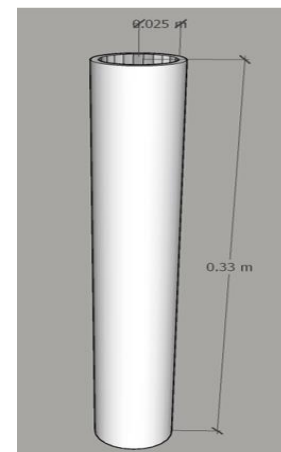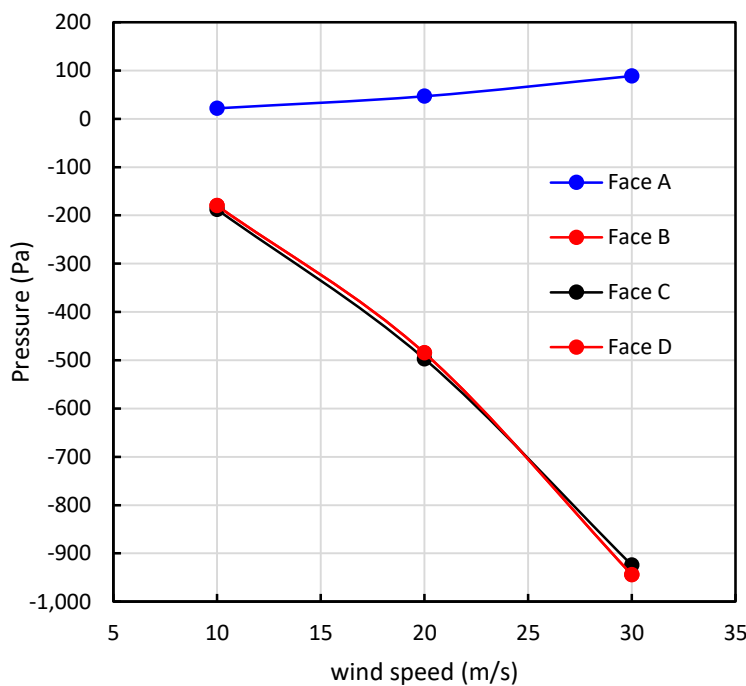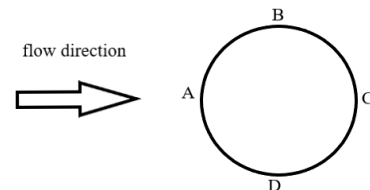
Figure 12 Pressure variation around building model A-1 for different wind speed

For the circular cross section with rib (A-2) the measured pressure values are tabulated in Table 5 for the three wind speeds 10, 20 and 30 m/s. Figure 13 shows the variation of surface pressure at the four sides with the variation in wind speed. The pressure at the upstream surface is almost changes with wind speed only and does not change with building model shape. Addition of the ribs around the circular cross section building model works on increasing the pressure on the sides and rear of the building. This reduces the difference in pressure between the upper and downstream of the building and consequently decreases the drag force on the building model.

Table 5 surface pressure variation with wind speed for model A-2

Wind velocity (m/sec)	Pressure (Pa)			
	Front A	Side B	Rear C	Side D
10	23	-175	-179	-175
20	48	-471	-488	-471
30	90	-940	-921	-940
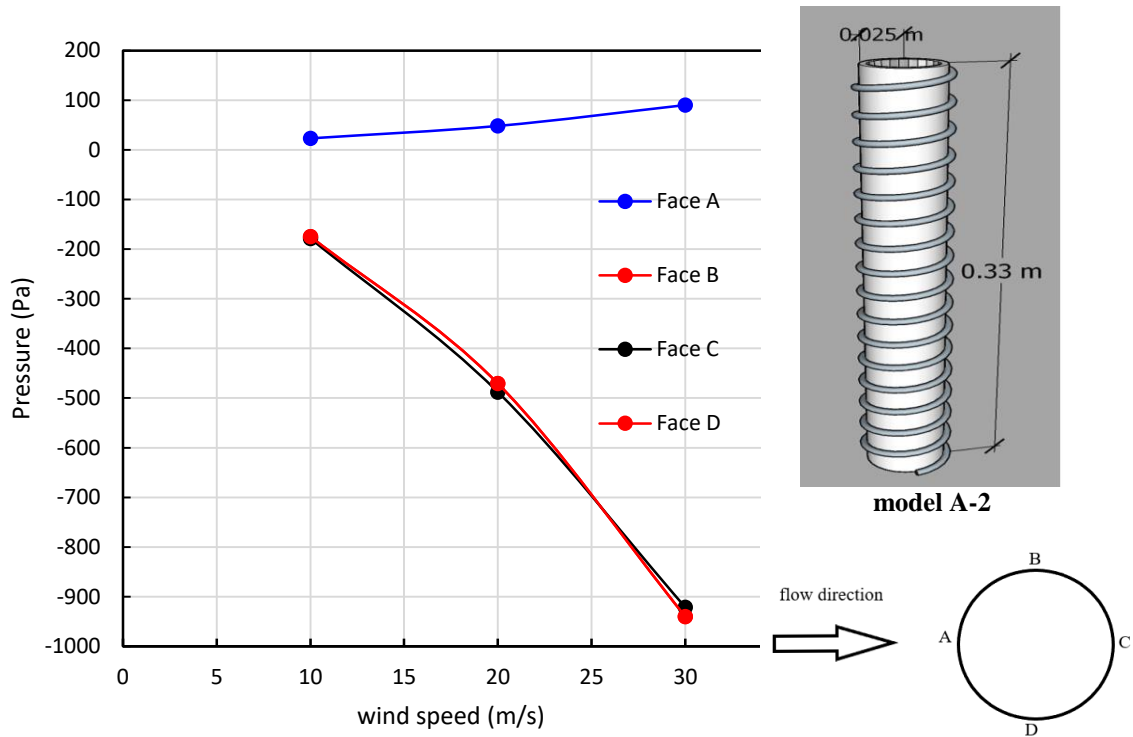
Figure 13 Pressure variation around building model A-2 for different wind speed

The measured surface pressure values are presented in Table 6 and Table 7 for rectangular and rectangular with curved nose respectively. The measurements were conducted at the three wind speeds 10, 20 and 30 m/s. Figure 14 and Figure 15 shows the measured pressure on the building surfaces variation at the four sides with wind speed for the rectangular cross section building model B-1. A little increase in the stagnation pressure is observed compared to circular cross section. The stagnation pressure decreases by using rectangular with curved nose.

Table 6 surface pressure variation with wind speed for model B-1

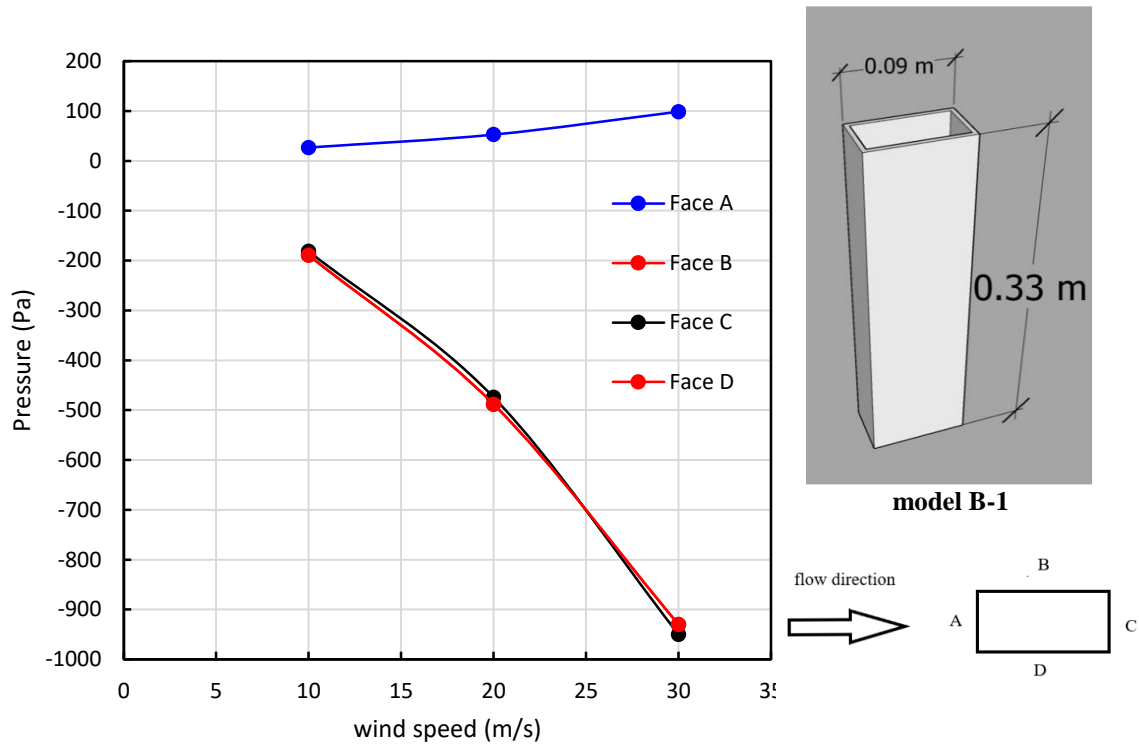| Wind velocity (m/sec)	Pressure (Pa)			
	Front A	**Side B**	**Rear C**	**Side D**
10	30	-188	-198	-188
20	67	-471	-479	-471
30	119	-894	-951	-894

Figure 14 Pressure variation around building model B-1 for different wind speed

Table 7 surface pressure variation with wind speed for model B-2

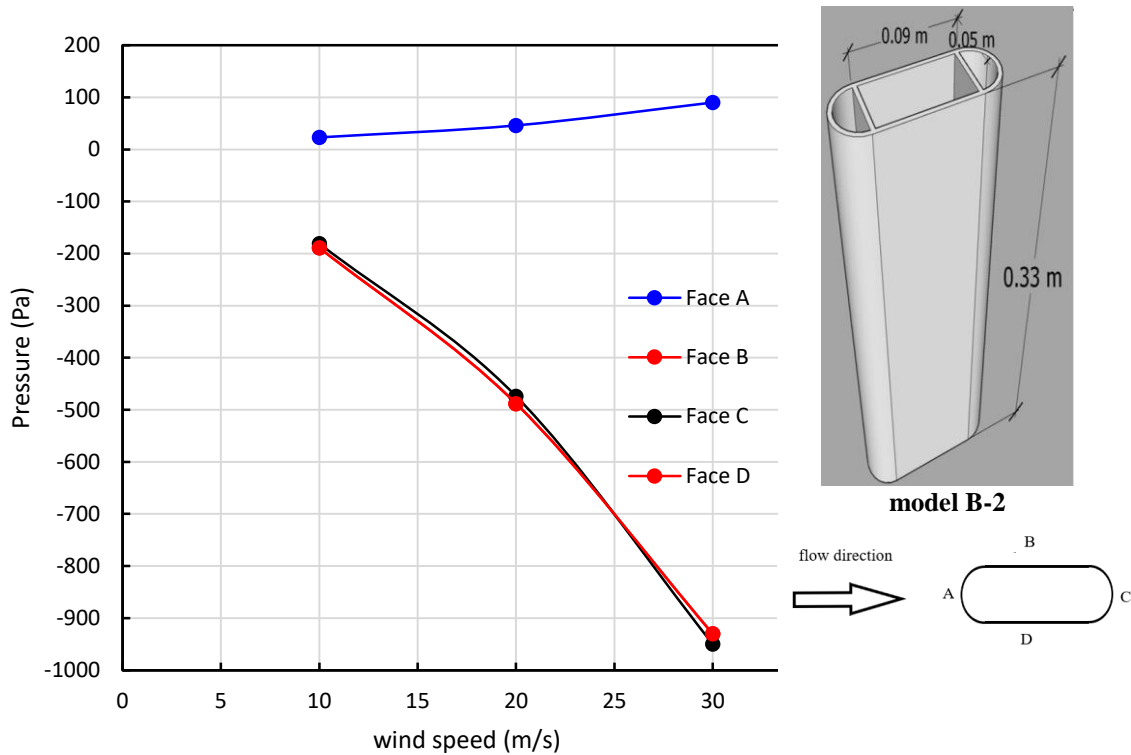| Wind velocity (m/sec)	Pressure (Pa)			
	Front A	**Side B**	**Rear C**	**Side D**
10	23	-189	-181	-189
20	46	-488	-475	-488
30	90	-930	-950	-930

Figure 15 Pressure values around building model B-2 cross section for different wind speed

The square cross section represents the traditional tall building. The measured surface pressure values are presented in Table 8 and Table 9 for square C and twisted E models respectively. The measurements were conducted at the three wind speeds 10, 20 and 30 m/s. Figure 16 and Figure 17 shows the measured pressure on the building surfaces variation at the four sides with wind speed for the square C and twisted E models respectively. Decrease in the stagnation pressure is observed due to twist compared to square cross section. The stagnation pressure decreases by using rectangular with curved nose. Table 13 presents the measured surface pressure values for curved surfaces model D. the results indicated that curved surfaces building shape gives a better distribution of pressure around building compared to twist E and rectangular with curved nose B-2. So, while selecting the building cross section shape it is recommended to use curved surfaces model D to decrease drag on the building, decrease pressure distribution effect and improve the side ventilation according to reduce the eddies effects. Figure 18 shows the measured pressure on the building surfaces variation at the four sides with wind speed for the curved surfaces model D.

Table 8 surface pressure variation with wind speed for model C

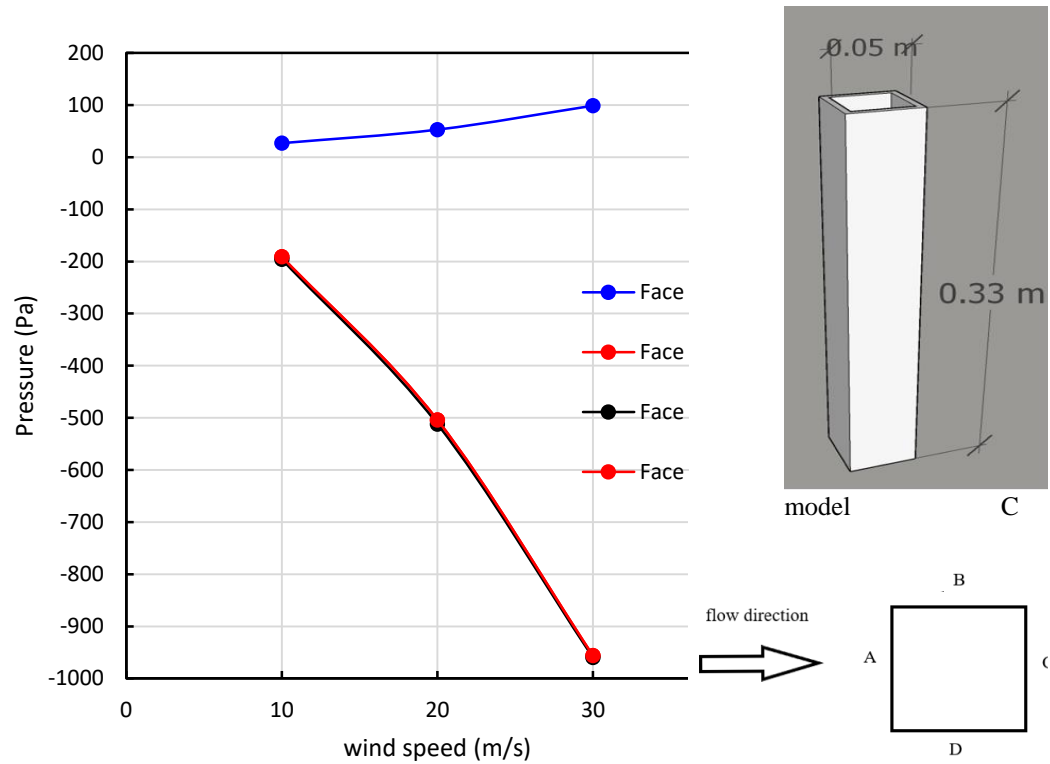| Wind velocity (m/sec)	Pressure (Pa)			
	Front A	Side B	Rear C	Side D
10	27	-191	-196	-191191
20	53	-504	-512	-504
30	99	-956	-960	-956

Figure 16 Pressure values around building model C cross section for different wind speed

Table 9 surface pressure variation with wind speed for model E

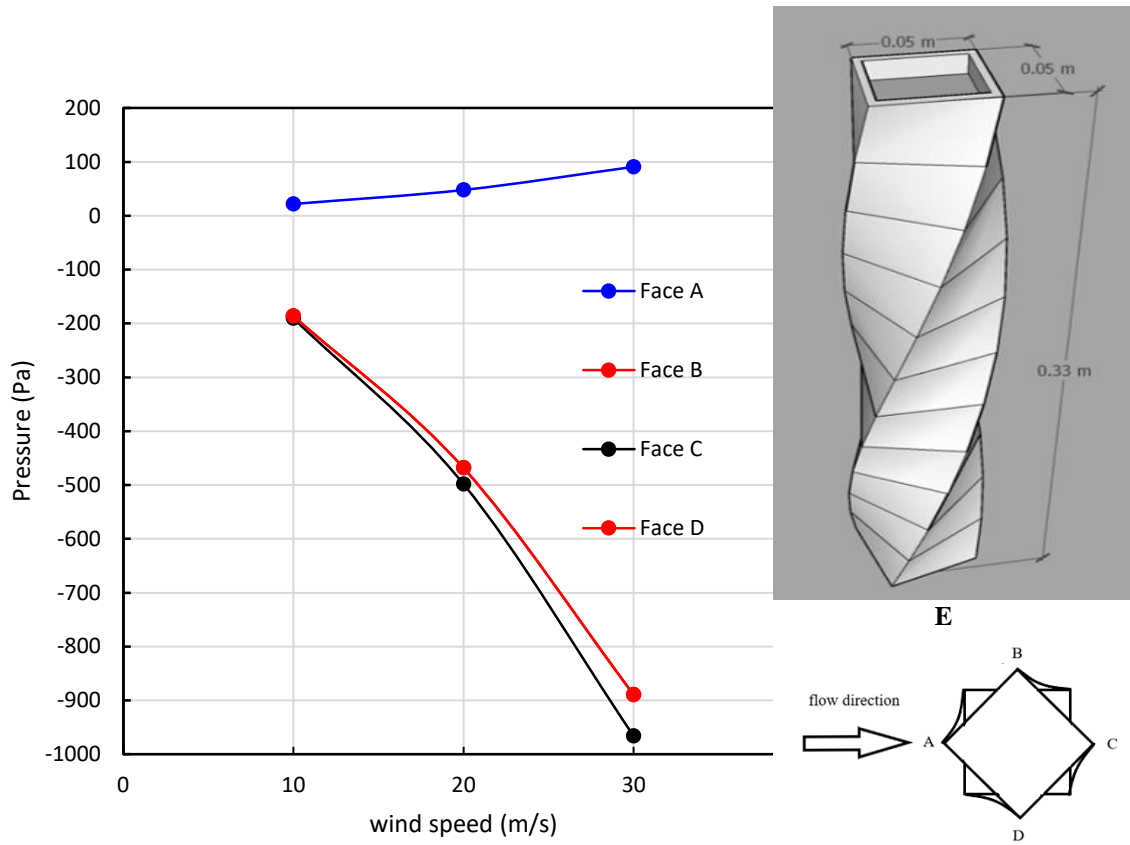| Wind velocity (m/sec)	Pressure (Pa)			
	Front A	Side B	Rear C	Side D
10	22	-186	-190	-184
20	48	-468	-498	-472
30	91	-889	-966	-893

Figure 17 Pressure values around building model E cross section for different wind speed

Table 10 surface pressure variation with wind speed for model D

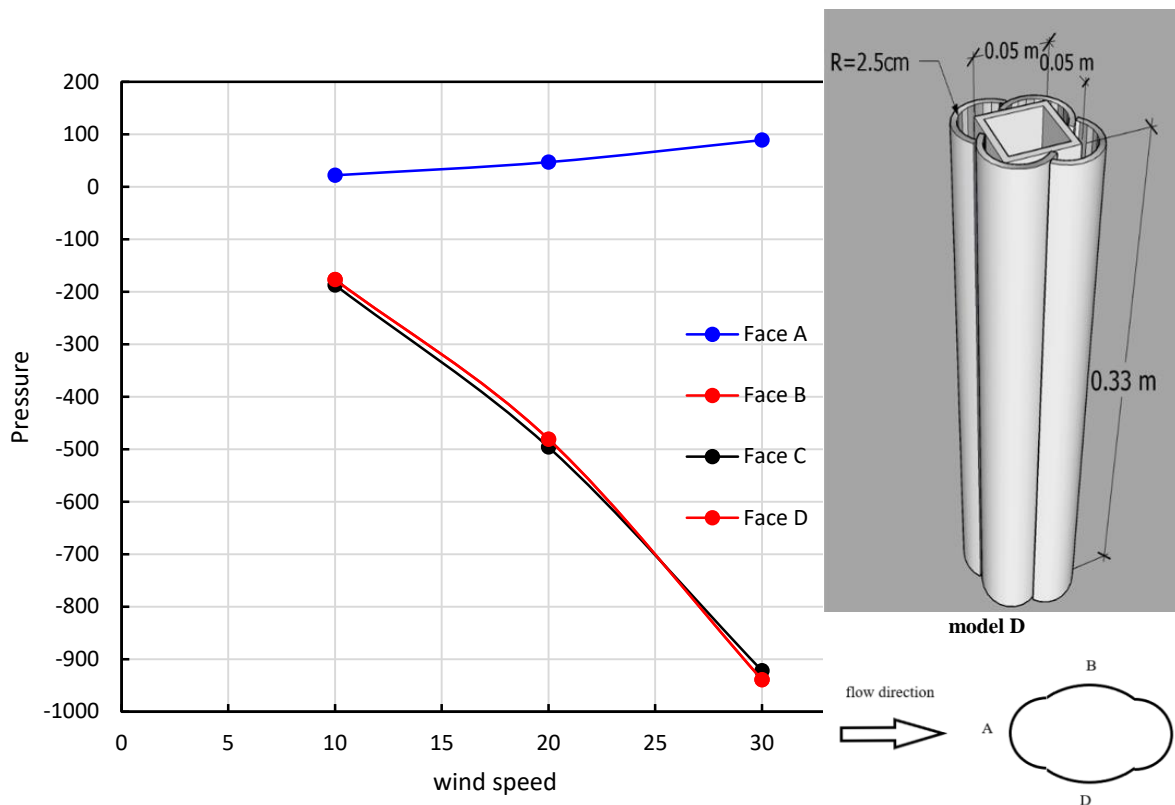| Wind velocity (m/sec)	Pressure (Pa)			
	Front A	Side B	Rear C	Side D
10	22	-177	-187	-177
20	47	-481	-496	-481
30	89	-939	-922	-939

Figure 18 Pressure values around building model D cross section for different wind speed

V. Conclusion

A 8 shapes of tall buildings models are used in present work to study the aerodynamic effect through measuring and visualization of important aerodynamic parameters and flow around the models. The study gives a simulation of different cross section of building models at three different wind speeds 10, 20 and 30 m/s.

1- As the wind speed increases, the pressure at stagnation point for the upstream surface also increases.
2- As the difference in pressure values between the upstream and downstream increase for the drag force on the building model increase also.
3- The eddies zone width behind the building model equal to 2.8d, 1.8d, 3.25d, 2.4d and 1.0d for A-1, A-2, C, E and D respectively where d equals 5 cm. The size and location of the eddies around the building models responsible for the building ventilation movements.
4- The modification of circular building model A-1 by using circular with helical rips model A-2 reduce the drag force.
5- The modification of rectangular building model B-1 by using rectangular with curved nose model B-2 reduce the drag force
6- The modification of square building model C by using twisted model E reduce the drag force by 21.32 %
7- The modification of square building model C by using curved surfaces model D reduce the drag force by 33 %

The data set that created by experimental tests on different building models based on ANN success to predict the effects on skyscrapers before starting by 99% depends on wind speed map history.

References

[1]. Kang, T. H. K., Martin, R. D., Park, H. G., Wilkerson, R., & Youssef, N. (2013). Tall Building With Steel Plate Shear Walls Subject To Load Reversal. The Structural Design Of Tall And Special Buildings, 22(6), 500-520. Https://Doi.Org/10.1002/Tal.700
[2]. Alinejad, H., & Kang, T. H. K. (2020). Engineering Review Of ASCE 7-16 Wind-Load Provisions And Wind Effect On Tall Concrete-Frame Buildings. Journal Of Structural Engineering, 146(6), 04020100. Https://Doi.Org/10.1061/(ASCE)ST.1943-541X.0002622
[3]. Elshaer, A., Bitsuamlak, G., & El Damatty, A. (2015, June). Aerodynamic Shape Optimization For Corners Of Tall Buildings Using CFD. In 14th International Conference On Wind Engineering (ICWE).
[4]. Mashalkar, B. S., Patil, G. R., & Jadhav, A. S. (2015). Effect Of Plan Shapes On The Response Of Buildings Subjected To Wind Vibrations. IOSR Journal Of Mechanical And Civil Engineering (IOSR-JMCE), 1, 80-89.
[5]. Thordal, M. S., Bennetsen, J. C., Capra, S., Kragh, A. K., & Koss, H. H. H. (2020). Towards A Standard CFD Setup For Wind Load Assessment Of High-Rise Buildings: Part 2–Blind Test Of Chamfered And Rounded Corner High-Rise Buildings. Journal Of Wind Engineering And Industrial Aerodynamics, 205, 104282. Https://Doi.Org/10.1016/J.Jweia.2020.104282

[6]. Roy, K. And Bairagi, A.K. (2016), "Wind Pressure And Velocity Around Stepped Unsymmetrical Plan Shape Tall Building Using CFD Simulation - A Case Study", Asian J. Civil Eng. Build. Housing, 17(8).

[7]. Meng, F.Q., He, B.J., Zhu, J., Zhao, D.X., Darko, A. And Zhao, Z. Q. (2018), "Sensitivity Analysis Of Wind Pressure Coefficients On CAARC Standard Tall Buildings In CFD Simulations", J. Build. Eng., 16, 146-158.

[8]. Chakraborty, S., Dalui, S.K. And Ahuja, A.K. (2014), "Wind Load On Irregular Plan Shaped Tall Building-A Case Study", Wind Struct, 19(1), 59-73.

[9]. Amin, J.A. And A.K. Ahuja (2010), "Aerodynamic Modifications To The Shape Of The Buildings: A Review Of The State-Of-The-Art.", Asian J. Civil Eng., (Build. Housing), 11(4).

[10]. Lin, N., Letchford, C., Tamura, Y., Liang, B. And Nakamura, O. (2005), "Characteristics Of Wind Forces Acting On Tall Buildings", J. Wind Eng. Ind. Aerod., 93(3), 217-242. Https://Doi.Org/10.1016/J.Jweia.2004.12.001

[11]. Elshaer, A., Gairola, A., Adamek, K. And Bitsuamlak, G. (2017), "Variations In Wind Load On Tall Buildings Due To Urban Development", Sustain. Cities Soc., 34, 264-277. Https://Doi.Org/10.1016/J.Scs.2017.06.008

[12]. Boonyapinyo, V. And Wangkansirikun, P. (2016), "Aerodynamic Modifications Of High-Rise Buildings For Wind Load And Response Reductions", In The 2016 International Conference On Advances In Wind And Structures (AWAS16).

[13]. Elnimeiri, M. And Mahsa N. (2011), "A Design Optimization Workflow For Tall Buildings Using Parametric Algorithm", CTBUH Conference, Seoul, October.

[14]. Jafari, M. And Alipour, A. (2021), "Methodologies To Mitigate Wind-Induced Vibration Of Tall Buildings: A State-Of-The-Art Review", J. Build. Eng., 33, 101582. Https://Doi.Org/10.1016/J.Jobe.2020.101582

[15]. Hui, Y., Tamura, Y., Yoshida, A., & Kikuchi, H. (2013). Pressure And Flow Field Investigation Of Interference Effects On External Pressures Between High-Rise Buildings. Journal Of Wind Engineering And Industrial Aerodynamics, 115, 150-161. Https://Doi.Org/10.1016/J.Jweia.2013.01.012

[16]. Agarwal, N., Mittal, A.K., And Gupta, V.K. (2012). "Along Wind Interference Effects On Tall Buildings." VI National Conference Of Wind Engineering, December 14-15.

[17]. Nagar1a, S. K., Raj, R., & Dev2b, N. (2020). Experimental Study Of Wind-Induced Pressures On Tall Buildings Of Different Shapes. Wind And Structures, 31(5), 441-453. Https://Doi.Org/10.12989/Was. 2020.31.5.441

[18]. Kwok, K. C. S. (1988). Effect Of Building Shape On Wind-Induced Response Of Tall Building. Journal Of Wind Engineering And Industrial Aerodynamics, 28(1-3), 381-390.Https://Doi.Org/10.1016/0167-6105(88)90134-1

[19]. Blessmann, J., & Riera, J. D. (1985). Wind Excitation Of Neighbouring Tall Buildings. Journal Of Wind Engineering And Industrial Aerodynamics, 18(1), 91-103. Https://Doi.Org/10.1016/0167-6105(85)90076-5

[20]. Chen, F. B., Wang, X. L., Li, X., Shu, Z. R., & Zhou, K. (2022). Prediction Of Wind Pressures On Tall Buildings Using Wavelet Neural Network. Journal Of Building Engineering, 46, 103674. Https://Doi.Org/10.1016/J.Jobe.2021.103674

[21]. Lin, P., Ding, F., Hu, G., Li, C., Xiao, Y., Tse, K. T., ... & Kareem, A. (2022). Machine Learning-Enabled Estimation Of Crosswind Load Effect On Tall Buildings. Journal Of Wind Engineering And Industrial Aerodynamics, 220, 104860. Https://Doi.Org/10.1016/J.Jweia.2021.104860

[22]. Holman, J. P. (2021). Experimental Methods For Engineers EIGHTH EDITION., Https://Doi.Org/10.1016/J.Rser.2018.03.026.